Transverse energy per charged particle at relativistic energies from a statistical model with expansion

Dariusz Prorok
Institute of Theoretical Physics, University of Wrocław,
Pl.Maksa Borna 9, 50-204 Wrocław, Poland
(Dated: September 15, 2004)

Transverse energy and charged particle pseudorapidity densities at midrapidity and their ratio, $dE_T/d\eta\ |_{mid}\ /dN_{ch}/d\eta|_{mid}$, are evaluated in a statistical model with longitudinal and transverse flows for the wide range of colliders, from AGS to RHIC at $\sqrt{s_{NN}} = 200$ GeV. Evaluations are done at freeze-out parameters established independently from fits to observed particle yields and p_T spectra. Decays of hadron resonances are treated thoroughly and are included in derivations of $dE_T/d\eta|_{mid}$ and $dN_{ch}/d\eta|_{mid}$. The predictions of the model agree well with the experimental data. However, some (explicable) overestimation of the ratio has been observed.

PACS numbers: 25.75.-q, 25.75.Dw, 24.10.Pa, 24.10.Jv

I. INTRODUCTION

In this paper, the idea of an independent test of the applicability of a statistical model for the description of the soft part of particle production in a heavy-ion collision postulated in [1], is developed for the much more realistic case of a hadron gas and its expansion. So far, the statistical model has been applied successfully in description of particle yield ratios and p_T spectra measured in heavy-ion collisions [2, 3, 4, 5, 6, 7, 8, 9, 10, 11, 12, 13, 14, 15] (there are also computation packages for thermal studies available from the Web [16, 17]). Now, the freeze-out parameters obtained from those analyses will be used to evaluate global observables: the transverse energy density $dE_T/d\eta$, the charged particle multiplicity density $dN_{ch}/d\eta$ and their ratio. The advantage of such an approach is based on the fact that transverse energy measurements are independent of hadron spectroscopy (in particular, no particle identification is necessary), therefore they could be used as an additional test of the self-consistency of a statistical model. The same holds true for the charged particle multiplicity, which actually is the charged *hadron* multiplicity, according to the experimental definition given in [18].

The experimentally measured transverse energy is defined as

$$E_T = \sum_{i=1}^{L} \hat{E}_i \cdot \sin\theta_i \ , \tag{1}$$

where θ_i is the polar angle, $\hat{E}_i$ denotes $E_i - m_N$ (m_N means the nucleon mass) for baryons and the total energy E_i for all other particles, and the sum is taken over all L emitted particles [19]. Additionally, in the case of RHIC at $\sqrt{s_{NN}} = 200$ GeV, $E_i + m_N$ is taken instead of E_i for antibaryons [20].

The statistical model with single freeze-out is used (for details see [13] and references therein). The model reproduces very well ratios and p_T spectra of particles measured at RHIC [9, 10, 11]. The main assumption of the model is the simultaneous occurrence of chemical and thermal freeze-outs, which is important if p_T spectra are considered (this enables to neglect the possible elastic interactions after the chemical freeze-out). Since in the present paper the integrated quantities over p_T are dealt with, the above-mentioned assumption should not be so important for final results.

The actually detected (stable) particles have two sources: (a) a thermal gas and (b) secondaries produced by decays and sequential decays of primordial resonances. All stable hadrons and confirmed resonances up to a mass of 2 GeV from the Particle Data Tables [21] are constituents of the gas. The distributions of particles from source (a) are given by a Bose-Einstein or a Fermi-Dirac distribution at the freeze-out. The distributions of secondaries (source (b)) can be obtained from the elementary kinematics of a many-body decay or from the superposition of two or more such decays (for details see the Appendix and [13]). In the following, all possible (2-, 3- and 4-body) decays with branching ratios not less than 1% are considered. Also almost all possible sequential decays are taken into account, namely: $2\circ2$, $2\circ2\circ2$, $2\circ2\circ2\circ2$, $2\circ3$, $2\circ4$, $3\circ2$, $3\circ3$, $2\circ2\circ3$, $2\circ3\circ2$, $3\circ2\circ2$, $2\circ3\circ3$, where 2, 3 and 4 mean the 2-, 3- and 4-body decay respectively, and a cascade proceeds from the right to the left (as in the usual mathematical definition of the superposition of functions). It should be stressed that all contributions from weak decays are included. The contribution to the transverse energy from the omitted cascades has been estimated at 0.2%. But since the most of these cascades ends with two photons, they do not contribute to the charged particle multiplicity at all.

II. THE BASIS OF THE FREEZE-OUT MODEL

The following are the foundations of the model. A noninteracting gas of stable hadrons and resonances at chemical and thermal equilibrium is created at the Central Rapidity Region (CRR) of a collision. The gas cools and expands, and after reaching the freeze-out point it ceases. The conditions for the freeze-out are expressed by values of two independent thermal parameters: the temperature T and the baryon number chemical potential μ_B. The strangeness chemical potential μ_S is determined from the requirement that the overall strangeness of the gas equals zero.

A freeze-out hypersurface is defined by the condition

$$\tau = \sqrt{t^2 - r_x^2 - r_y^2 - r_z^2} = const \ , \tag{2}$$

which means that the freeze-out takes place at a fixed moment of the invariant time τ. Additionally, it is assumed that the four-velocity of an element of the freeze-out hypersurface is proportional to its coordinate,

$$u^\mu = \frac{x^\mu}{\tau} = \frac{t}{\tau} \ \left(1, \frac{r_x}{t}, \frac{r_y}{t}, \frac{r_z}{t}\right) \ . \tag{3}$$

Then the following parameterization of the hypersurface is chosen:

$$t = \tau \cosh\alpha_\parallel \cosh\alpha_\perp, \quad r_x = \tau \sinh\alpha_\perp \cos\phi, \quad r_y = \tau \sinh\alpha_\perp \sin\phi, \quad r_z = \tau \sinh\alpha_\parallel \cosh\alpha_\perp, \tag{4}$$

where $\alpha_\parallel$ is the rapidity of the element, $\alpha_\parallel = \tanh^{-1}(r_z/t)$, and $\alpha_\perp$ determines the transverse radius

$$r = \sqrt{r_x^2 + r_y^2} = \tau \sinh\alpha_\perp. \tag{5}$$

To keep the transverse size finite, r is restricted by the condition $r < \rho_{max}$. In this way one has two additional parameters of the model, τ and ρ_{max}, connected with the geometry of the freeze-out hypersurface.

Also the transverse velocity, v_ρ, can be obtained

$$v_\rho = \sqrt{\left(\frac{r_x}{t}\right)^2 + \left(\frac{r_y}{t}\right)^2} = \frac{\tau \sinh\alpha_\perp}{t} = \frac{\tanh\alpha_\perp}{\cosh\alpha_\parallel} = \frac{\beta_\perp}{\cosh\alpha_\parallel} \ , \tag{6}$$

which is the value of the transverse velocity $\beta_\perp$ from the central slice after boosting it in the longitudinal direction. The transverse velocity can be expressed as a function of the transverse radius

$$\beta_\perp(r) = \tanh\alpha_\perp = \frac{r}{\sqrt{\tau^2 + r^2}} \ . \tag{7}$$

Since it is an increasing function of r, the maximum value of $\beta_\perp$ called the maximum transverse-flow parameter (or the surface velocity), is given by

$$\beta_\perp^{max} = \frac{\rho_{max}}{\sqrt{\tau^2 + \rho_{max}^2}} = \frac{\rho_{max}/\tau}{\sqrt{1 + (\rho_{max}/\tau)^2}} \ , \tag{8}$$

so it depends only on the ratio ρ_{max}/τ.

III. TRANSVERSE ENERGY AND CHARGED PARTICLE DENSITIES

According to the general description founded in [22] and developed in [10, 11] for the case with decays taken into account, the invariant distribution of the measured particles of species i has the form

$$\frac{dN_i}{d^2p_T \ dy} = \int p^\mu d\sigma_\mu \ f_i(p \cdot u) \ , \tag{9}$$

where $d\sigma_\mu$ is the normal vector on a freeze-out hypersurface, $p \cdot u = p^\mu u_\mu$, u_μ is the four-velocity of a fluid element and f_i is the final momentum distribution of the particle in question. The final distribution means here that f_i is the sum of primordial and simple and sequential decay contributions to the particle distribution (for details see [13]). For the hypersurface and expansion described in sect. II, eq. (9) takes the following form:

$$\frac{dN_i}{d^2p_T\ dy} = \tau^3 \int\limits_{-\infty}^{+\infty} d\alpha_\parallel \int\limits_0^{\rho_{max}/\tau} \sinh\alpha_\perp d(\sinh\alpha_\perp) \int\limits_0^{2\pi} d\xi\ p\cdot u\ f_i(p\cdot u)\ , \tag{10}$$

where

$$p\cdot u = m_T \cosh\alpha_\parallel \cosh\alpha_\perp - p_T \cos\xi \sinh\alpha_\perp\ . \tag{11}$$

Note that the distribution expressed by eqs. (10) and (11) is explicitly boost invariant (in fact, it is constant with respect to rapidity).

The rapidity density of particle species i is given by

$$\frac{dN_i}{dy} = \int d^2p_T\ \frac{dN_i}{d^2p_T\ dy}\ , \tag{12}$$

whereas the corresponding pseudorapidity density reads

$$\frac{dN_i}{d\eta} = \int d^2p_T\ \frac{dy}{d\eta}\ \frac{dN_i}{d^2p_T\ dy} = \int d^2p_T\ \frac{p}{E_i}\ \frac{dN_i}{d^2p_T\ dy}\ . \tag{13}$$

Analogously, the transverse energy pseudorapidity density for the same species can be written as

$$\frac{dE_{T,i}}{d\eta} = \int d^2p_T\ \hat{E}_i\cdot\frac{p_T}{p}\ \frac{dy}{d\eta}\ \frac{dN_i}{d^2p_T\ dy} = \int d^2p_T\ p_T\ \frac{\hat{E}_i}{E_i}\ \frac{dN_i}{d^2p_T\ dy}\ . \tag{14}$$

For the quantities at midrapidity one has

$$\frac{dN_i}{d\eta}\Big|_{mid} = \int d^2p_T\ \frac{dN_i}{d^2p_T\ dy}\ \frac{\sqrt{p_T^2 + v_{c.m.s}^2 m_i^2}}{m_T}\ , \tag{15}$$

$$\frac{dE_{T,i}}{d\eta}\Big|_{mid} = \begin{cases} \int d^2p_T\ p_T\ \frac{dN_i}{d^2p_T\ dy}\ \frac{m_T - \sqrt{1-v_{c.m.s}^2}m_N}{m_T}, i = nucleon \\ \int d^2p_T\ p_T\ \frac{dN_i}{d^2p_T\ dy}, i \neq nucleon\ . \end{cases} \tag{16}$$

where $v_{c.m.s}$ is the velocity of the center of mass of two colliding nuclei with respect to the laboratory frame (only for RHIC $v_{c.m.s} = 0$). For RHIC at $\sqrt{s_{NN}} = 200$ GeV the case $i \neq nucleon$ in eq. (16) is replaced by

$$\frac{dE_{T,i}}{d\eta}\Big|_{mid} = \begin{cases} \int d^2p_T\ p_T\ \frac{dN_i}{d^2p_T\ dy}\ \frac{m_T + m_N}{m_T}, i = antinucleon \\ \int d^2p_T\ p_T\ \frac{dN_i}{d^2p_T\ dy}, i \neq nucleon,\ antinucleon\ . \end{cases} \tag{17}$$

Now, the overall charged particle and transverse energy densities can be obtained

$$\frac{dN_{ch}}{d\eta}\Big|_{mid} = \sum_{i\in B} \frac{dN_i}{d\eta}\Big|_{mid}\ , \tag{18}$$

$$\frac{dE_T}{d\eta}\Big|_{mid} = \sum_{i\in A} \frac{dE_{T,i}}{d\eta}\Big|_{mid}\ , \tag{19}$$

where A and B ($B \subset A$) denote sets of species of finally detected particles. In the view of the definition given in [18] and the detailed description of the experimental setup and the analysis procedure from [23], the set of charged particles B can consist of stable hadrons only, $B = \{\pi^+,\ \pi^-,\ K^+,\ K^-,\ p,\ \bar{p}\}$, whereas A also includes photons, K_L^0, n and $\bar{n}$ [19].

TABLE I: Comparison of the statistical model estimates of the rapidity densities of charged particles with the experimental values for the 5% most central collisions at $\sqrt{s_{NN}} = 130$ GeV at RHIC [24].

Particles	$dN_{ch}/dy\|_{y=0}$	
	Theory	Experiment
$\pi^+ + \pi^-$	548.6	546 ± 54.5
$K^+ + K^-$	84.6	87.2 ± 12.0
$p + \bar{p}$	55.8	48.8 ± 6.2

IV. RESULTS

To check the self-consistency of the described model, rapidity densities of pions, kaons, protons and antiprotons have been calculated for the 5% most central Au-Au collisions at $\sqrt{s_{NN}} = 130$ GeV at RHIC. The supplied values of the thermal and geometric parameters are in this case $T = 165$ MeV, $\mu_B = 41$ MeV, $\tau = 8.2$ fm and $\rho_{max} = 6.9$ fm [9, 13]. The geometric parameters were obtained from the fit to the p_T spectra of the above-mentioned particles [24]. The integrated yields over p_T are also given in [24], so the comparison with the predictions of eq. (12) can be done easily. The results are presented in TABLE I. Note that the very good agreement has been found.

The presentation of the main results of the paper needs a few comments concerning the AGS case. In the all cited papers the same method of establishing the thermal parameters T and μ_B is applied. The method is based on the best fit of calculated particle density ratios to the relative particle abundance data. But the different model of the freeze-out was applied for the description of p_T spectra measured at AGS [2, 5]. In that model (for details see [25]), the freeze-out happens instantaneously in the r direction, *i.e.* at a constant value of t (*not* at a constant value of τ as here). The shape of a hypersurface in the longitudinal direction is not determined explicitly, but due to the factorization of the transverse mass spectrum it can affect only the normalization. The parameters connected with the expansion are the surface velocity $\beta_\perp^{max}$ and ρ_{max}. The transverse velocity profile has the following form

$$\beta_\perp(r) = \beta_\perp^{max} \left(\frac{r}{\rho_{max}} \right)^\alpha , \tag{20}$$

with the choice $\alpha = 1$. Therefore, the implementation of values of $\beta_\perp^{max}$ obtained within that model into the presented one is entirely *ad hoc*, nevertheless it works surprisingly well. Of course, one directly could apply the description of the transverse flow from [25] to calculate the transverse energy and charged particle densities, but it is much more tempting and elegant to work within one model. Additionally, there is one technical problem connected with the treatment of resonance decays. Here, the very convenient form of the invariant distribution, eq. (9), has been derived because the normal vector is proportional to the four-velocity, $d\sigma_\mu \propto u_\mu$. This is not the case for the hypersurface chosen in [25], so the calculation of resonance decay contributions would be much more complex (for the exact formulae, see [13]). Note also that in the view of [26], particle distributions depend very weakly on the exact form of the velocity profile (*i.e.* for considered $\alpha = 0.5,\ 1$, and 2) in the model described in [25]. It can be checked that profile (7) lies in between two profiles of the form (20) with $\alpha = 0.5$, and 1.

To put values of $\beta_\perp^{max}$ from [2, 5] into formulae of sect. III, one should invert eq. (8) to obtain

$$\frac{\rho_{max}}{\tau} = \frac{\beta_\perp^{max}}{\sqrt{1 - (\beta_\perp^{max})^2}} . \tag{21}$$

It should be recalled here, that the value of τ itself is not necessary to calculate the transverse energy per charged particle, since this parameter cancels in the ratio.

The final results of numerical estimates of $dE_T/d\eta|_{mid}$ and $dN_{ch}/d\eta|_{mid}$ together with the corresponding experimental data are listed in TABLE II. To make predictions for the AGS case it has been assumed that the maximal

TABLE II: Values of $dE_T/d\eta|_{mid}$ and $dN_{ch}/d\eta|_{mid}$ calculated in the framework of the statistical model with expansion. In the first column thermal and geometric parameters are listed for the corresponding collisions. In the third and last column experimental data for the most central collisions are given.

Collision case	$dE_T/d\eta\|_{mid}$ [GeV]		$dN_{ch}/d\eta\|_{mid}$	
	Theory	Experiment	Theory	Experiment
Au-Au at RHIC at $\sqrt{s_{NN}} = 200$ GeV:				
$T = 165.6$ MeV, $\mu_B = 28.5$ MeV	585 [a]	597 ± 34 [20]	589	699 ± 46 [20]
$\rho_{max} = 7.15$ fm, $\tau = 7.86$ fm ($\beta_\perp^{max} = 0.67$) [12]				579 ± 29 [b] [30]
Au-Au at RHIC at $\sqrt{s_{NN}} = 130$ GeV:				
$T = 165$ MeV, $\mu_B = 41$ MeV	507	503 ± 25 [19]	555	622 ± 41 [23]
$\rho_{max} = 6.9$ fm, $\tau = 8.2$ fm ($\beta_\perp^{max} = 0.64$) [13]				568 ± 47 [b] [24]
Pb-Pb at SPS:				
$T = 164$ MeV, $\mu_B = 234$ MeV	447	363 ± 91 [27]	476	464^{+20}_{-13} [27]
$\rho_{max} = 6.45$ fm, $\tau = 5.74$ fm ($\beta_\perp^{max} = 0.75$) [14, 15]				
Au-Au at AGS:				
$T = 130$ MeV, $\mu_B = 540$ MeV	224	≈ 200 [28]	271	≈ 270 [29]
$\beta_\perp^{max} = 0.675$, $\rho_{max} = 6.52$ fm [2, 5]				
Si-Pb at AGS:				
$T = 120$ MeV, $\mu_B = 540$ MeV	57	≈ 62 [29]	91	$\approx 115 - 120$ [29]
$\beta_\perp^{max} = 0.54$, $\rho_{max} = 5.02$ fm [2, 5]				

[a] For the modified definition of E_T, *i.e.* $E_i + m_N$ is taken instead of E_i for antibaryons, see eq. (1).
[b] For the charged particle multiplicity expressed as the sum of integrated charged hadron yields.

transverse size ρ_{max} equals the average of radii of two colliding nuclei and the nucleus radius has been expressed as $R_A = r_0 A^{\frac{1}{3}}$, $r_0 = 1.12$ fm. Generally, the overall agreement is good. For RHIC the $11\% - 16\%$ underestimation of the charged particle density has been received ($5\% - 10\%$ with respect to the lowest allowed values). But this result simply reflects the existing inconsistency in measurements of the charged particle multiplicity at RHIC. Namely, the sum of integrated charged hadron yields (see TABLE I), after converting to $dN_{ch}/d\eta$ [20], is substantially less then the directly measured $dN_{ch}/d\eta|_{mid}$. This is shown explicitly in the last column of TABLE II. For RHIC at $\sqrt{s_{NN}} = 130$ GeV, the sum is 8.7% smaller then the total charged particle multiplicity. For RHIC at $\sqrt{s_{NN}} = 200$ GeV it is even worse, the sum is about 17% below the total $dN_{ch}/d\eta|_{mid}$. But both values of the sum agree very well with the model predictions. Since the geometric parameters were established from the fits to the same p_T spectra, the agreement had to be obtained. Also for AGS the results agree qualitatively well with the data, in spite of the roughness of the method applied for this case. The overall error of evaluations of transverse energy and charged particle densities is about 0.5% and has two origins: (a) omission of the most complex cascades; (b) simplifications in numerical procedures for more involved cascades. The velocity of the center of mass of two colliding nuclei, $v_{c.m.s}$, equals: 0 for RHIC, 0.994 for SPS Pb-Pb collisions at $158 \cdot A$ GeV, 0.918 for AGS Au-Au collisions at $11 \cdot A$ GeV and 0.678 for AGS Si-Pb collisions at $14.6 \cdot A$ GeV.

Values of the ratio $dE_T/d\eta|_{mid}/dN_{ch}/d\eta|_{mid}$ can be also given. They are collected in TABLE III, together with the corresponding data. Generally, the overall overestimation of the order of 15% has been obtained. In the RHIC case this is the result of the underestimation of $dN_{ch}/d\eta|_{mid}$, which has been explained earlier. But when in the denominator of the experimental ratio, $dN_{ch}/d\eta|_{mid}$ from the summing up of integrated hadron yields is put, the theoretical predictions agree very well with the data. Note that the similar inconsistency in charged particle measurements could have also been the origin of the discrepancy between model and experimental values of $dN_{ch}/d\eta|_{mid}$ seen in the AGS Si-Pb case. For SPS, the result agrees with the experimental value within errors. The overall error of model evaluations of the ratio is less than 1%. These results have been also depicted together with the data in fig. 1. One can see that the relative positions of theoretical points agree very well with the data, they are shifted up only and this is the effect of the overestimation discussed earlier.

It should be stressed that $dE_T/d\eta|_{mid}/dN_{ch}/d\eta|_{mid}$ depends substantially on the value of $\beta_\perp^{max}$. It can be seen

TABLE III: Values of the ratio $dE_T/d\eta|_{mid}/dN_{ch}/d\eta|_{mid}$ calculated in the framework of the statistical model with expansion. In the last column experimental data for the most central collisions are given.

Collision case	$dE_T/d\eta\|_{mid}/dN_{ch}/d\eta\|_{mid}$ [GeV]	
	Theory	Experiment
Au-Au at RHIC at $\sqrt{s_{NN}} = 200$ GeV	0.99 [a]	0.87 ± 0.06 [20] 1.03 ± 0.08 [b]
Au-Au at RHIC at $\sqrt{s_{NN}} = 130$ GeV	0.91	0.81 ± 0.06 [19] 0.89 ± 0.09 [b]
Pb-Pb at SPS	0.94	0.78 ± 0.21 [27]
Au-Au at AGS	0.83	0.72 ± 0.08 [29]
Si-Pb at AGS	0.63	0.52-0.54 [29]

[a] For the modified definition of E_T, *i.e.* $E_i + m_N$ is taken instead of E_i for antibaryons, see eq. (1).
[b] Author calculations with the use of experimental values given in TABLE II and the denominator expressed as the sum of integrated charged hadron yields.

TABLE IV: Dependence of the transverse energy per charged particle on the maximum transverse-flow parameter $\beta_\perp^{max}$ for Au-Au collisions at AGS.

$\beta_\perp^{max}$	$dE_T/d\eta\|_{mid}/dN_{ch}/d\eta\|_{mid}$ [GeV]
0.4	0.61
0.57	0.72
0.675	0.83
0.8	1.07

from TABLE IV, where the transverse energy per charged particle estimates have been listed for a few values of $\beta_\perp^{max}$ for Au-Au collisions at AGS. Having compared with the experimental data (see TABLE III), one can notice that this model yields the value of $\beta_\perp^{max}$ which is slightly lower than the value obtained within the model described in [25].

V. COMPARISON WITH A STATIC CASE

It would be very interesting to check how expansion influences the transverse energy per charged particle. The expansion produces additional energy so this process should increase the energy of a particle emitted from a thermal source. The preliminary analysis of a static case was done in [1]. But to compare with the present results up-to-date calculations should be performed. In [1] a gas with only 40 species (including antiparticles) was examined and feeding charged particles from weak decays of neutral resonances was excluded. Thus, to extract the expansion contribution to $dE_T/d\eta|_{mid}/dN_{ch}/d\eta|_{mid}$ one has to apply the general scheme of sect. III again, but with the proper replacement of the invariant particle distribution.

For a static gas (*static* in the c.m.s, of course), the invariant distribution of the measured particles of species i has

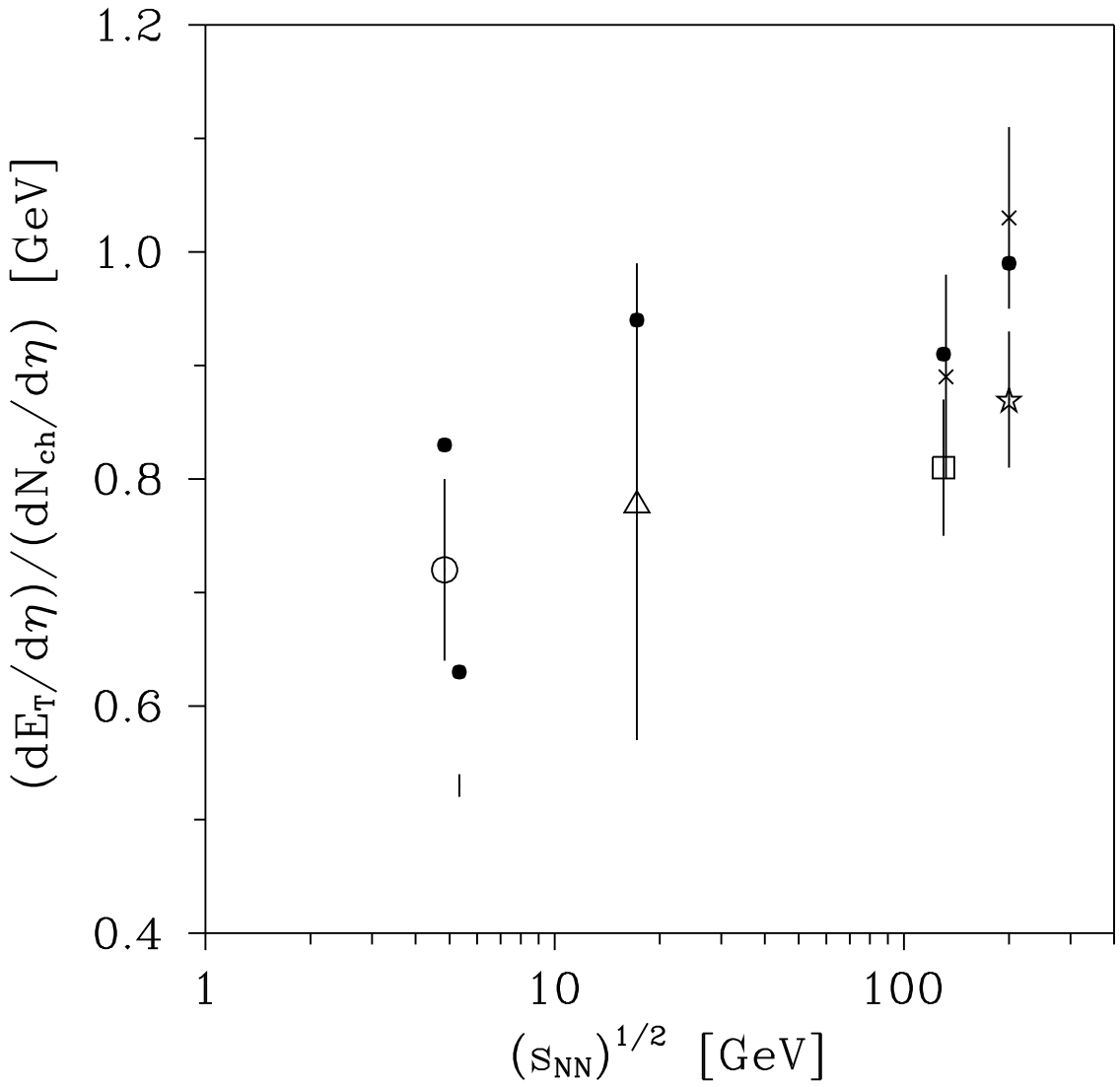

FIG. 1: Values of the transverse energy per charged particle at midrapidity for the most central collisions. Black dots denote evaluations of the ratio in the framework of the present model (the second column of TABLE III). Also data points for AGS [29] (a circle for Au-Au and a vertical bar for Si-Pb), SPS [27] (triangle), RHIC at $\sqrt{s_{NN}} = 130$ GeV [19] (square) and RHIC at $\sqrt{s_{NN}} = 200$ GeV [20] (star) are depicted. For RHIC, points with the sum of integrated charged hadron yields substituted for the denominator are also depicted (crosses).

the form [1]

$$\frac{dN_i}{d^2p_T\ dy} = V^*\ E_i^*\ f_i(E_i^*)\ , \tag{22}$$

where E_i^* is the c.m.s energy of the ith particle and V^* denotes the c.m.s volume of the gas at the freeze-out. Thus, at midrapidity, one has:

$$\frac{dN_i}{d^2p_T\ dy}\ \Big|_{mid} = V^*\ m_T\ f_i(m_T)\ . \tag{23}$$

Now the general formulae of eqs. (15)-(19) can be applied, but with dN_i/d^2p_Tdy given by eq. (23) instead of eq. (10). The results of numerical evaluations of $dE_T/d\eta|_{mid}/dN_{ch}/d\eta|_{mid}$ for the static gas are collected in TABLE V. In this case only two (thermal) parameters are needed and they are the same as in TABLE II. Having compared with

TABLE V: Values of the ratio $dE_T/d\eta|_{mid}/dN_{ch}/d\eta|_{mid}$ calculated for the static gas. In the last column experimental data for the most central collisions are given.

Collision case	$dE_T/d\eta\|_{mid}/dN_{ch}/d\eta\|_{mid}$ [GeV]	
	Theory	Experiment
Au-Au at RHIC at $\sqrt{s_{NN}} = 200$ GeV	0.89 [a]	0.87 ± 0.06 [20]
Au-Au at RHIC at $\sqrt{s_{NN}} = 130$ GeV	0.82	0.81 ± 0.06 [19]
Pb-Pb at SPS	0.71	0.78 ± 0.21 [27]
Au-Au at AGS	0.62	0.72 ± 0.08 [29]
Si-Pb at AGS	0.53	0.52-0.54 [29]

[a]For the modified definition of E_T, *i.e.* $E_i + m_N$ is taken instead of E_i for antibaryons, see eq. (1).

TABLE III, one can see that expansion is responsible for the following increases of the transverse energy per charged particle: 11% for RHIC, 32% for SPS, 34% for AGS Au-Au collisions and 19% for AGS Si-Pb collisions. This can be explained reasonably. The transverse energy per charged particle has two contributions: the first thermal and the second originated from expansion. The first is governed mainly by the temperature and the second by the maximum transverse-flow parameter $\beta_\perp^{max}$. For a given temperature, the increase of $\beta_\perp^{max}$ should cause the weighting of the expansion contribution. But for a constant value of $\beta_\perp^{max}$, the strengthening of this contribution can be maintained by the lowering of the temperature. This is why for almost the same $\beta_\perp^{max}$ (see the first column of TABLE II) the relative growth of the transverse energy per charged particle, after switching the expansion on, is much greater for AGS Au-Au collisions than for RHIC ones. On the other hand, for comparable temperatures, the expansion contributes to the transverse energy per charged particle much stronger for SPS than for RHIC (the former has substantially greater $\beta_\perp^{max}$).

VI. CONCLUSIONS

The expanding thermal hadron gas model has been used to reproduce transverse energy and charged particle multiplicity pseudorapidity densities and their ratio measured at AGS, SPS and RHIC. The importance of the present analysis originates from the fact that the transverse energy and the charged particle multiplicity are *independent observables*, so they can be used as new tools to verify the consistency of predictions of a statistical model for all colliders simultaneously. The predictions have been made at the previous estimates of thermal and geometric freeze-out parameters obtained from analyses of measured particle ratios and p_T spectra at AGS [2, 5], SPS [14, 15] and RHIC [12, 13]. The overall good agreement, not only of the ratio but also absolute values of $dE_T/d\eta\ |_{mid}$ and $dN_{ch}/d\eta|_{mid}$, with the data has been achieved. And the observed discrepancies can be explained reasonably. This strongly supports the idea that the thermal expanding source is responsible for the soft part of the particle production in heavy-ion collisions. Moreover, the description of various observables is consistent within one statistical model.

In fact, there are additional arguments which make the above statement even more valuable. In principle, one could think at first glance that this analysis is nothing more like a kind of an internal consistency check of various measurements. And such a check could be done even in an model-independent way simply by integrating spectra of stable particles (the first time with the expression for transverse energy to obtain $dE_T/d\eta\ |_{mid}$ and the second time without, to receive $dN_{ch}/d\eta|_{mid}$) and then adding them all. But there are two reasons that this can not be done without any external input. First, transverse momentum spectra are measured in *limited ranges*, so very important low-p_T regions are not covered by the data. For instance at RHIC, the first point for pions is at $p_T = 0.25$ GeV/c, for kaons at $p_T = 0.45$ GeV/c and for protons and antiprotons at $p_T = 0.65$ GeV/c [24, 30]. There are also upper limits, but contributions from ranges above them are suppressed strongly in comparison with the low-p_T regions. Therefore,

to obtain integrated yields some extrapolations below and above the measured ranges are used. Usually two functions are used for each species and the contributed value is the average of their integrals. In fact these extrapolations are only analytical fits without any physical reasoning, but, for instance, contributions from regions covered by them account for 30% of the yield for pions, 40% for kaons and 25% for protons and antiprotons for RHIC at $\sqrt{s_{NN}} = 130$ GeV [24]. On the other hand, a calorimeter acts very effectively for these species in the low-p_T range, namely pions with $p_T \leq 0.35$ GeV/c, kaons with $p_T \leq 0.64$ GeV/c and protons and antiprotons with $p_T \leq 0.94$ GeV/c deposit all their kinetic energy [19]. Since the very accurate predictions for the transverse energy density at midrapidity have been obtained (see TABLE II), the present analysis can be understood as an undirect proof that in these unmeasurable p_T regions spectra are also explicable by means of the thermal source with flow and decays.

Second, it is impossible to check the consistency of the transverse energy data because not all stable hadron spectra are measured at midrapidity for each collision case. This mainly concerns neutrons and K^0_L. The lacking contribution from hadron decay photons could be approximated to some extent with the use of π^0 and η spectra, but they are also limited in ranges. And again, the very good agreement of model estimates of the transverse energy density at midrapidity with the data can be interpreted as the strong argument that the production of neutral stable particles can be described in terms of the expanding thermal source with superimposed decays.

And last but not least, in opposite to the transverse energy, there is some inconsistency (of the order of 10%) of the independent measurements of charged particle multiplicities with the corresponding sums of integrated charged particle yields at RHIC (see sect. IV). However, only for the case of $\sqrt{s_{NN}} = 200$ GeV the substantial gap (of the order of 6% with respect to the direct measurement) between error bars of these two differently obtained values of $dN_{ch}/d\eta|_{mid}$ exists. For the case of $\sqrt{s_{NN}} = 130$ GeV the error bars overlap almost one half of each other. But since the data at $\sqrt{s_{NN}} = 200$ GeV are still preliminary, it is difficult to judge whether this inconsistency has the physical or experimental (an additional systematic error?) reason.

The role of expansion is substantial. It produces about $10\% - 30\%$ of the transverse energy per charged particle. But, as can be seen from TABLE V, the expansion is not necessary to explain the experimental data for $dE_T/d\eta\ |_{mid}$ $/dN_{ch}/d\eta|_{mid}$. The results suggest that the most of the transverse energy per charged particle is produced by the thermal movement. For sure, the expansion is necessary to explain the absolute values of $dE_T/d\eta\ |_{mid}$ and $dN_{ch}/d\eta|_{mid}$. To obtain these one needs a volume of a place of "action" and the most adequate way to do it is to parameterize the evolution of the system in space and time, that is to put the expansion in.

As the last comment, it should be stressed that the results of the present paper have been obtained within the model where the chemical freeze-out happens simultaneously with the thermal one. However, so far the most extensively studied scenario is that where the thermal freeze-out occurs later then the chemical freeze-out (for a review, see [31] and references therein). This problem has not been addressed here. But one should notice that the distinction between these two freeze-outs means the introduction of the next parameter (the fifth here) into the model. Of course, an extra parameter in a phenomenological model always causes (or at least should cause) better agreement with the data. At the present level of investigations both spectra (refs. [10, 11, 15]) and global observables $dE_T/d\eta\ |_{mid}$ and $dN_{ch}/d\eta|_{mid}$ (this analysis) are predicted accurately with the assumption of the one freeze-out. However, more detailed studies should be performed to check whether the transverse energy per charged particle measurement could help somehow in distinction or not between these two freeze-outs and this will be the subject of further investigations.

Acknowledgments

The author gratefully acknowledges very stimulating discussions with Wojciech Broniowski and Wojciech Florkowski. He also thanks Ludwik Turko for careful reading of the manuscript and Anna Jadczyk for help in preparing the LaTeX 2_εfile. This work was supported in part by the Polish Committee for Scientific Research under Contract No. KBN 2 P03B 069 25.

APPENDIX

The derivation of the momentum distribution of a product of a two-body decay $M \longrightarrow m_1 + m_2$ can be found in [32] or [9]. For an n-body decay $M \longrightarrow m_1 + m_2 + ... + m_n$, the momentum distribution of the product (labeled 1) can be written (following the method presented in [9]) as:

$$f_1^{(n)}(|\vec{q}|, M, m_1, m_2, ..., m_n) \ = \ B\frac{2s_M + 1}{2s_1 + 1}\frac{1}{N^{(n)}(M; m_1, m_2, ..., m_n)}\int d^3\vec{k} f_M(|\vec{k}|)$$

$$\times \int \left(\prod_{i=1}^{n} \frac{d^3\vec{p}_i}{E_i} \right) \delta(M - \sum_{i=1}^{n} E_i) \delta^{(3)}(\sum_{i=1}^{n} \vec{p}_i)$$
$$\times \delta^{(3)}(\hat{L}_{\vec{k}} \vec{p}_1 - \vec{q}) \, , \tag{A.1}$$

where

$$\hat{L}_{\vec{k}} \vec{p}_1 = \vec{p}_1 + \left\{ (\gamma_k - 1) \frac{\vec{p}_1 \cdot \vec{k}}{k^2} + \frac{E_1}{M} \right\} \vec{k} \, , \tag{A.2}$$

$$\gamma_k = \frac{E_M}{M} \, , \quad E_M = \sqrt{M^2 + \vec{k}^2} \, , \quad E_i = \sqrt{m_i^2 + \vec{p}_i^{\,2}} \, , \tag{A.3}$$

and s_M (s_1) is the spin of the resonance (the product), B is the branching ratio, $f_M(|\vec{k}|)$ denotes the momentum distribution of the decaying resonance and $N^{(n)}$ is the corresponding phase-space integral:

$$N^{(n)}(M; m_1, m_2, ..., m_n) = \int \left(\prod_{i=1}^{n} \frac{d^3\vec{p}_i}{E_i} \right) \delta(M - \sum_{i=1}^{n} E_i) \delta^{(3)}(\sum_{i=1}^{n} \vec{p}_i) \, . \tag{A.4}$$

The invariant amplitude for the decay, $\mathcal{M}$, is assumed to be a constant here, so $|\mathcal{M}|^2$ cancels during normalization.

With the use of the well-known technique of splitting up the phase-space integral into a convolution integral over two phase-space integrals (here, the first responsible for the 2-body decay and the second representing the $(n-1)$-body decay) [32], the following recursive formulae for the n-body decay can be derived:

$$\begin{aligned} f_1^{(n)}(|\vec{q}|, M, m_1, m_2, ..., m_n) \; &= \; B \frac{2s_M + 1}{2s_1 + 1} \frac{2\pi}{N^{(n)}(M; m_1, m_2, ..., m_n)} \frac{1}{qE_1(q)} \\ &\times \int\limits_{m_2 + ... + m_n}^{M - m_1} dm \; m N^{(n-1)}(m; m_2, ..., m_n) \\ &\times \int\limits_{k_-(q; M, m_1, m)}^{k_+(q; M, m_1, m)} dk \; k \; f_M(k) \, , \end{aligned} \tag{A.5}$$

$$N^{(n)}(M; m_1, m_2, ..., m_n) = \frac{4\pi}{M} \int\limits_{m_2 + ... + m_n}^{M - m_1} dm \; m \; N^{(n-1)}(m; m_2, ..., m_n) \; p(M; m_1, m) \, , \tag{A.6}$$

where

$$k_\pm(q; M, m_1, m_2) = \frac{M}{m_1^2} |p(M; m_1, m_2) E_1(q) \pm q E(M; m_1, m_2)| \, , \tag{A.7}$$

for $m_1 \neq 0$, whereas

$$\begin{cases} k_+(q; M, m_1, m_2) = +\infty, \\ k_-(q; M, m_1, m_2) = \frac{|\frac{1}{4}(M^2 - m_2^2)^2 - M^2 q^2|}{(M^2 - m_2^2) q} \end{cases} \tag{A.8}$$

for $m_1 = 0$, and

$$p(M; m_1, m_2) = \frac{M}{4\pi} N^{(2)}(M; m_1, m_2) = \frac{\sqrt{[M^2 - (m_1 + m_2)^2][M^2 - (m_1 - m_2)^2]}}{2M} \, , \tag{A.9}$$

$$E(M; m_1, m_2) = \frac{M^2 - m_2^2 + m_1^2}{2M} \, . \tag{A.10}$$

[1] D. Prorok, Acta Phys. Polon. B **34**, 4219 (2003).
[2] P. Braun-Munzinger, J. Stachel, J. P. Wessels and N. Xu, Phys. Lett. B **344**, 43 (1995).
[3] P. Braun-Munzinger, J. Stachel, J. P. Wessels and N. Xu, Phys. Lett. B **365**, 1 (1996).
[4] J. Cleymans, D. Elliott, H. Satz and R. L. Thews, Z. Phys. C **74**, 319 (1997).
[5] J. Stachel, Nucl. Phys. A **610**, 509C (1996).
[6] P. Braun-Munzinger, I. Heppe and J. Stachel, Phys. Lett. B **465**, 15 (1999).
[7] F. Becattini, J. Cleymans, A. Keranen, E. Suhonen and K. Redlich, Phys. Rev. C **64**, 024901 (2001).
[8] P. Braun-Munzinger, D. Magestro, K. Redlich and J. Stachel, Phys. Lett. B **518**, 41 (2001).
[9] W. Florkowski, W. Broniowski and M. Michalec, Acta Phys. Polon. B **33**, 761 (2002).
[10] W. Broniowski and W. Florkowski, Phys. Rev. Lett. **87**, 272302 (2001).
[11] W. Broniowski and W. Florkowski, Phys. Rev. C **65**, 064905 (2002).
[12] A. Baran, W. Broniowski and W. Florkowski, Acta Phys. Polon. B **35**, 779 (2004).
[13] W. Broniowski, A. Baran and W. Florkowski, Acta Phys. Polon. B **33**, 4235 (2002).
[14] M. Michalec, Ph.D. thesis, arXiv:nucl-th/0112044.
[15] W. Broniowski and W. Florkowski, Acta Phys. Polon. B **33**, 1935 (2002).
[16] G. Torrieri, W. Broniowski, W. Florkowski, J. Letessier and J. Rafelski, arXiv:nucl-th/0404083.
[17] S. Wheaton and J. Cleymans, arXiv:hep-ph/0407174.
[18] B. B. Back *et al.* [PHOBOS Collaboration], Phys. Rev. Lett. **85**, 3100 (2000).
[19] K. Adcox *et al.* [PHENIX Collaboration], Phys. Rev. Lett. **87**, 052301 (2001).
[20] A. Bazilevsky [PHENIX Collaboration], Nucl. Phys. A **715**, 486 (2003).
[21] K. Hagiwara *et al.* [Particle Data Group Collaboration], Phys. Rev. D **66**, 010001 (2002).
[22] F. Cooper and G. Frye, Phys. Rev. D **10**, 186 (1974).
[23] K. Adcox *et al.* [PHENIX Collaboration], Phys. Rev. Lett. **86**, 3500 (2001).
[24] K. Adcox *et al.* [PHENIX Collaboration], Phys. Rev. Lett. **88**, 242301 (2002).
[25] E. Schnedermann, J. Sollfrank and U. Heinz, Phys. Rev. C **48**, 2462 (1993).
[26] S. Esumi, S. Chapman, H. van Hecke and N. Xu, Phys. Rev. C **55**, R2163 (1997).
[27] M. M. Aggarwal *et al.* [WA98 Collaboration], Eur. Phys. J. C **18**, 651 (2001).
[28] J. Barrette *et al.* [E814/E877 Collaboration], Phys. Rev. Lett. **70**, 2996 (1993).
[29] J. Barrette *et al.* [E877 Collaboration], Phys. Rev. C **51**, 3309 (1995).
[30] S. S. Adler *et al.* [PHENIX Collaboration], Phys. Rev. C **69**, 034909 (2004).
[31] U. W. Heinz, Nucl. Phys. A **661**, 140 (1999).
[32] R. Hagedorn, *Relativistic kinematics*, (W. A. Benjamin, Inc., Advanced Book Program, Reading, Massachusetts, Third printing, 1973).